CrossMark

RESEARCH ARTICLE

A semi-automated "blanket" method for renal segmentation from non-contrast T1-weighted MR images

Henry Rusinek[1] · Jeremy C. Lim[2] · Nicole Wake[1] · Jas-mine Seah[3] ·
Elissa Botterill[2] · Shawna Farquharson[4] · Artem Mikheev[1] · Ruth P. Lim[2,5]

Abstract

Objective   To investigate the precision and accuracy of a new semi-automated method for kidney segmentation from single-breath-hold non-contrast MRI.

Materials and methods   The user draws approximate kidney contours on every tenth slice, focusing on separating adjacent organs from the kidney. The program then performs a sequence of fully automatic steps: contour filling, interpolation, non-uniformity correction, sampling of representative parenchyma signal, and 3D binary morphology. Three independent observers applied the method to images of 40 kidneys ranging in volume from 94.6 to 254.5 cm^3. Manually constructed reference masks were used to assess accuracy.

Results   The volume errors for the three readers were: 4.4 % ± 3.0 %, 2.9 % ± 2.3 %, and 3.1 % ± 2.7 %. The relative discrepancy across readers was 2.5 % ± 2.1 %. The interactive processing time on average was 1.5 min per kidney.

Conclusions   Pending further validation, the semi-automated method could be applied for monitoring of renal status using non-contrast MRI.

✉ Henry Rusinek
  hr18@nyu.edu

[1] Center for Advanced Imaging Innovation and Research (CAI2R) and Department of Radiology, New York University School of Medicine, 660 1st Avenue, Rm413, New York, NY 10016, USA

[2] Radiology, Austin Health, Melbourne, VIC, Australia

[3] Endocrinology, Austin Health, Melbourne, VIC, Australia

[4] Florey Neuroscience Institute, Melbourne, VIC, Australia

[5] The University of Melbourne, Melbourne, VIC, Australia

Introduction

Kidney volume is an important measure for the early detection and monitoring of many renal diseases, including diabetic nephropathy, renal artery stenosis, graft assessment, and polycystic kidney disease [1]. While the mechanisms of volume changes are different in each disease, in most cases, progressive disease is characterized by eventual loss of parenchymal volume. In diabetic nephropathy, initial renal hypertrophy has been observed, particularly in patients with type 1 diabetes [2], and has been linked to poorer outcomes [3]. In patients with renovascular disease, volume is reduced with significant renal artery stenosis. Importantly, renal volume correlates significantly more closely with measured single-kidney glomerular filtration rate (GFR) than traditional 2D bipolar measurements [4], and can potentially predict how patients will respond to revascularization [5]. Increased renal volume, on the other hand, is a highly sensitive and specific marker of acute interstitial rejection for renal allografts [6]. Progression of polycystic kidney disease leads to the enlargement of kidney volume due to cyst formation [7], with higher volumes inversely related to GFR [8]. Renal volumes have potential application to kidney donor work-up, where they have shown stronger correlation with true measured GFR than serum GFR estimation [9]. Renal segmentation is also essential for functional renal assessment (renal perfusion and filtration) in dynamic contrast imaging [10].

MRI is an attractive modality for both structural and functional renal assessment [11]. MRI provides good tissue contrast without ionizing radiation exposure, and allows a
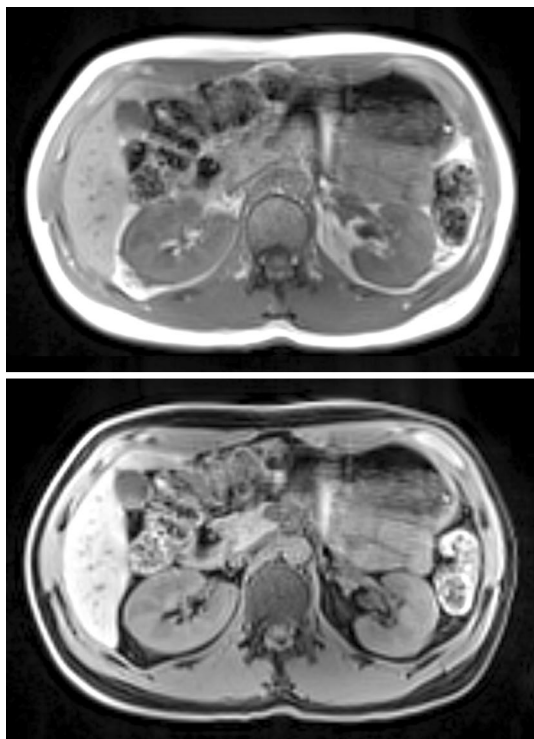
Fig. 1 A representative axial slice through the kidney before (*top*) and after (*bottom*) fat suppression. Note adjacent organs and skeletal muscle with MR signal similar to the kidney

highly flexible choice of protocols to probe not only single-kidney volume, but glomerular filtration, perfusion, oxygen content, and water diffusion parameters as well.

Fast T1-weighted (T1-W) gradient echo and 2D fast spin echo are the primary sequences used by radiologists to assess kidney disease. Dynamic functional imaging, which uses gadolinium contrast, is attractive for volumetric analysis, as it provides exquisite signal contrast. One drawback of segmentation from dynamic contrast-enhanced (DCE) images is that such DCE protocols emphasize temporal resolution at the cost of spatial resolution. To maximize segmentation accuracy, voxel size should be as small as possible. Modern technology allows an isotropic 1.5–2.0-mm T1-W renal acquisition within a single breath-hold. This is important in order to minimize motion artifacts that reduce image quality. Another well-known drawback to the use of contrast media, especially in patients with kidney insufficiency, is the potential nephrotoxic effect.

Despite providing a detailed depiction of a kidney, a fully automated renal segmentation from non-contrast MRI remains a challenge. The key difficulty is due to the closeness in gray level of the adjacent liver, spleen, vertebrae, and parts of the gastrointestinal tract that may be in contact with the kidney (Fig. 1). The problem increases in thin

patients because the fat surrounding the kidney is almost completely lacking. A recent study by Will et al. [12] demonstrates that borders between the kidney and the surrounding organs (spleen, gastrointestinal tract) can be identified with the use of a sophisticated post-processing algorithm and the assumption of the convexity for the kidney. However, this method requires the acquisition and co-registration of two complementary (T1-W and T2-W) data sets in separate breath-holds.

We have developed a semi-automated approach in which the human observer separates the kidney from the liver, spleen, and intestines. A unique aspect of our tool is that it is largely insensitive to inter-observer differences. The user input is effectively ignored over the ~90 % of the kidney surface that is not adjacent to the surrounding organs of similar signal. Briefly, the user draws over-inclusive approximate contours around the kidney on selected slices, focusing on separating organs immediately adjacent to the kidney. After this 1–2-min interaction, the program performs a sequence of automated steps that include non-uniformity correction, sampling of pure kidney signal, thresholding, and 3D binary morphology.

This segmentation technique was applied to non-contrast MRIs of healthy individuals and patients diagnosed with various stages of type 1 diabetes (T1DM). These patients were chosen because T1DM kidneys present with a wide range of volume, depending on the severity of diabetic nephropathy.

Renal segmentation is simplified by the fact that the kidney is immediately surrounded by a variable-thickness layer of perirenal fat. In addition, fatty tissue is present in the center of the kidney. Since hydrogen nuclei in water and fat have different resonance frequencies, the fat signal can be effectively suppressed (Fig. 1). We have applied this method to both T1-W and fat-suppressed data to examine whether fat suppression facilitates the task of kidney segmentation. To assess the accuracy of this segmentation technique, we used kidney reference masks constructed manually by a radiologist experienced in renal anatomy and renal disease. We measured inter-observer reliability of the segmentation and monitored the processing time. The accuracy of the segmentation tool was compared with a recently developed and publicly available tool, Robust Statistics Segmenter (RSS), based on the evolution of active contours [13].

Materials and methods

Study subjects

After procurement of informed consent and ethics institutional approval, abdominal images obtained from ten

Fig. 2 Observer selects for processing the inferior-most kidney slice (slice 2 in this example) and processes every tenth slice (2, 12, 22, 32, 42, and 52), always ending at the superior-most kidney slice. The goal is to separate the kidney from adjacent organs with signal intensity similar to that of the kidney. Enlarged slice 42 is on the *right*
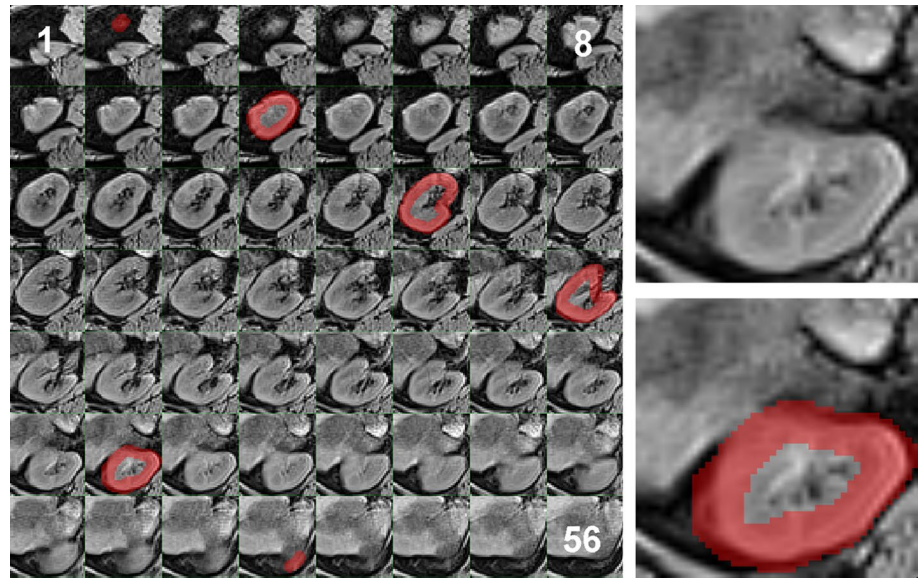
healthy volunteers (5 men, 5 women; mean age 43 years, range 28–63) and ten T1DM patients recruited to a study of early diabetic kidney disease (6 men, 4 women; mean age 50 years, range 29–74) were selected for volumetric analysis. A total of 40 kidneys (20 left, 20 right) were used. Images were de-identified prior to analysis, with readers blinded to patient identity and renal function.

MRI protocol

All images were acquired on 3T MRI (Skyra, Siemens, Erlangen, Germany) equipped with an 18-channel body phased-array coil anteriorly and 32-channel spine coil posteriorly. The anterior and posterior coil elements were selected by the radiographer to ensure optimal coil coverage for the region of interest. Volumetric interpolated breath-hold examination (VIBE) imaging was performed with a breath-hold at end-expiration: repetition time (TR) 3.8 ms, echo time (TE) 1.2 (out of phase) and 2.5 (in phase) ms, flip angle (FA) 9°, field of view (FOV) $384 \times 384 \times 208$ mm, true voxel size $2 \times 2 \times 3.8$ mm^3 interpolated to $2 \times 2 \times 2$ mm^3, acceleration factor 3 (GRAPPA), acquisition time 20 s. Integrated with VIBE is the Dixon technique based on chemical shift, or the difference in resonance frequencies between fat- and water-bound protons. Separate fat-only and water-only images were calculated by the system.

Blanket segmentation procedure

The segmentation process begins with the observer tracing over-inclusive kidney contours on a small subset of slices. Tracing was done on every s-th slice in the axial
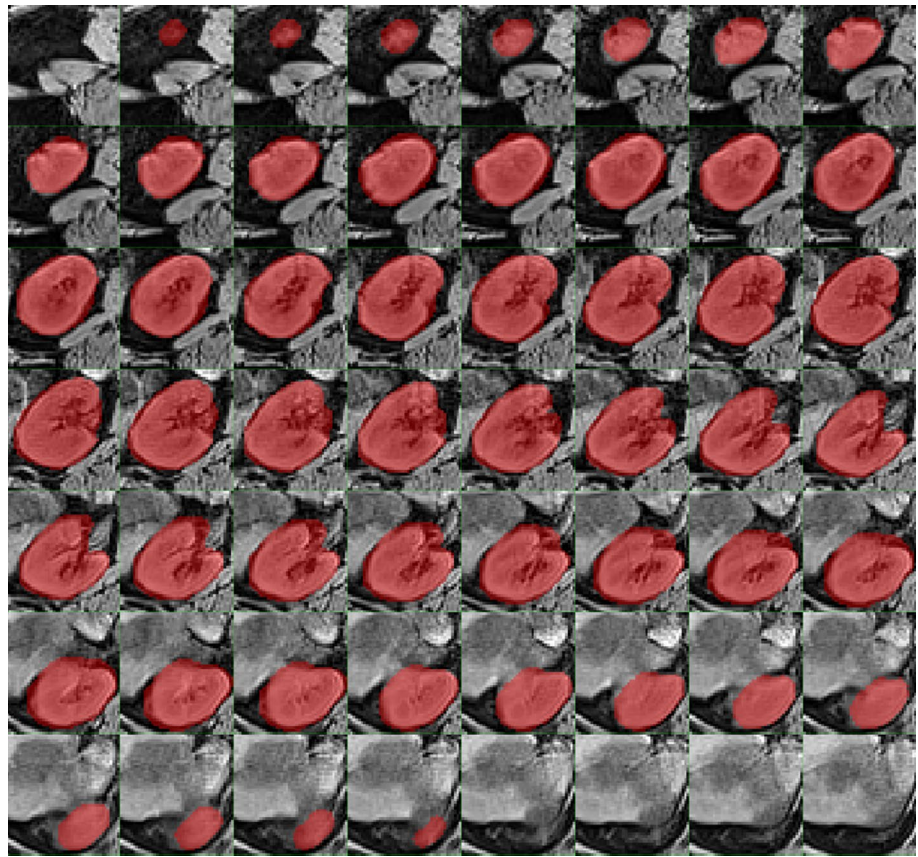
direction. An example of $s = 10$ is shown in Fig. 2 (see figure caption for details). Over-inclusive tracing is accomplished using an electronic paintbrush controlled by a computer mouse. Tracing is the only manual step in the segmentation process. To measure inter-observer reproducibility of the workflow, three independent observers independently drew the contours. The observers had 13, 5, and 1 year (R1, R2, R3) of experience with renal anatomy and abdominal imaging. Bland–Altman plots were used to analyze the agreement between pairs of observers.

The contours were morphologically filled [14] and interpolated in the z direction to yield the over-inclusive region we refer to as the "blanket" (Fig. 3). Interpolation of renal mask M_{start} on slice *zstart* and mask M_{end} on slice *zend* is accomplished by constructing a list $L[i]$ of all possible line segments connecting TRUE voxels from M_{start} to TRUE voxels in M_{end}. For each slice m between *zstart* and *zend*, we initialize the interpolated mask to FALSE. For each i, we then compute the coordinates (k, l) of the intersection of segment $L[i]$ with the plane of slice m; we then set voxel (k, l, m) to TRUE.

The desired properties of the blanket are that (1) the entire kidney is included, and (2) the liver, spleen, intestines, and tissue with signal intensity similar to that of the kidney are excluded. The goal of the subsequent segmentation process is to automatically trim from the blanket other non-renal tissue: perirenal and pelvic fat, collecting system, and blood vessels.

Let B_{xmin}, B_{xmax}, B_{ymin}, B_{ymax}, B_{zmin}, and B_{zmax} denote the minimum and maximum voxel coordinates of the blanket along the three spatial directions. In the next step, the program generates the bounding box defined as:

Fig. 3 Over-inclusive contours
after interior filling and *z*-axis
interpolation

$$\left\{ x, y, z : B_{x}\mathrm{min} - M < x < B_{x}\mathrm{max} + M \;\&\; B_{y}\mathrm{min} \right.$$
$$-M < y < B_{y}\mathrm{max} + M \& B_{z}\mathrm{min}$$
$$\left. -M < z < B_{z}\mathrm{max} + M \right\}$$

where *M* is a 10-mm margin. All subsequent processing is restricted to the bounding box.

In the next step, we apply non-uniformity correction to the bounding box. A well-validated *N3* algorithm is used [15]. The *N3* technique iteratively estimates a smooth multiplicative bias field that corrupts true scan intensities. We set *N3* to terminate at the 75th iteration and used 10-mm full width at half maximum (FWHM) for bias field smoothness—settings that have been used successfully in another segmentation task, the measurement of urine output through changes in bladder volume [16]. All subsequent steps were applied to the corrected image.

The program next finds a small three-dimensional "seed" sub-region of the kidney. The seed is a box-shaped region, D, of fixed dimensions $6 \times 6 \times 12$ mm, with the long dimension in the head–foot direction. The centroid of the seed is allowed to vary within 30 mm of the centroid of the blanket region. The seed location (Fig. 4) is selected to minimize the metric:

$$\frac{\max\limits_{(x,y,z)\in D} S(x, y, z) - \min\limits_{(x,y,z)\in D} S(x, y, z)}{\operatorname*{avg}\limits_{(x,y,z)\in D} S(x, y, z)}$$

over all potential seed locations, where *S* is the uniformity-corrected MR signal. The average seed signal S_0 is used for the initial intensity thresholding, generating the set V_0 of voxels:

$$V_0 = \{ v : S_0\, t_{low} < S(v) < S_0 t_{high} \},$$

where $S(v)$ is the signal intensity of voxel *v,* and t_{low} and t_{high} are dimensionless parameters determined relative to S_0. The parameter t_{low} directly affects inclusion/exclusion of partially volumed voxels at the edge of the kidney. Its value t_{low} was obtained from:

$$S_0\, t_{low} = 0.5\, (S_0 + B_0),$$

where B_0 is the representative background signal (from manual sampling). The goal is to retain in V_0 edge voxels containing >50 % of renal parenchyma. For our T1-W VIBE sequence, we estimated t_{low} to be 0.55.

The next step is to apply morphologic "peel" of V_0 obtained by eroding all voxels within a given distance *p* from the boundary of V_0. The result is decomposed into connected components. Only components that include the
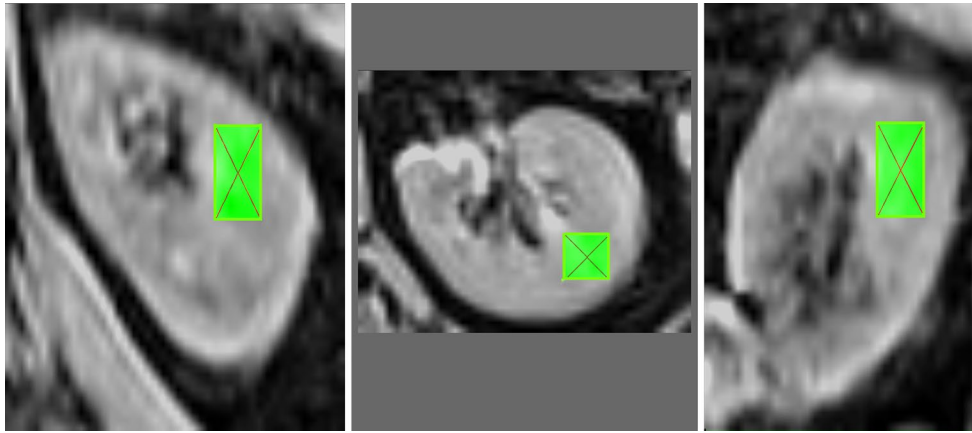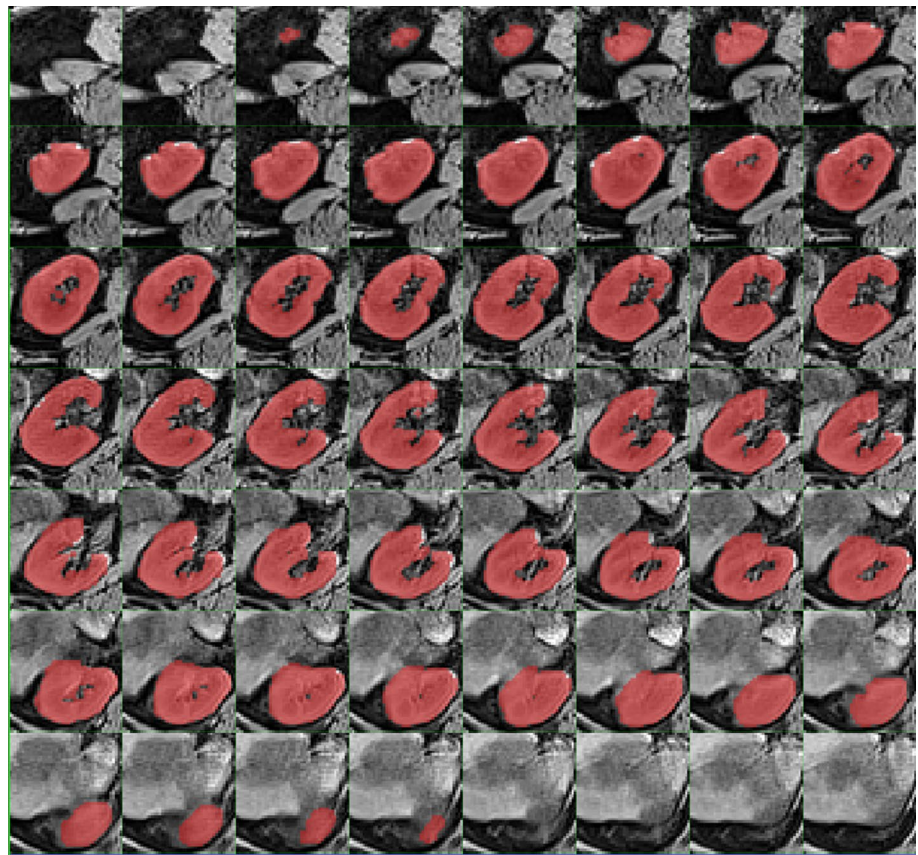
Fig. 4 Renal seed in coronal, axial, and sagittal views

Fig. 5 Final renal mask

seed are retained. We then apply the constrained morphologic growth operation [17] that aims to enlarge the eroded peeled set by re-including eroded voxels that must also be contained in the blanket region. One of the objectives of applying these morphologic operators (erosion, connected components, dilation by g, the growth radius) is to remove from V_0 thin structures which are presumed to be blood vessels and renal collecting system. A representative resulting renal mask is shown in Fig. 5. The segmentation program

(http://wp.nyu.edu/firevoxel) was implemented using the Visual Studio C++ compiler (Microsoft Corp, Redmond, WA, USA) for the Microsoft Windows operating system.

Robust Statistics Segmenter

The Robust Statistics Segmenter (RSS) algorithm, based on a variational framework [13], is included in the specialized segmentation module of the 3D Slicer 4.4 software package

Fig. 6 A representative kidney (*upper row*) with seed (*lower row*) drawn for Robust Statistics Segmenter. The seed consists of 3-mm-wide paintbrush strokes drawn in axial, sagittal, and coronal views
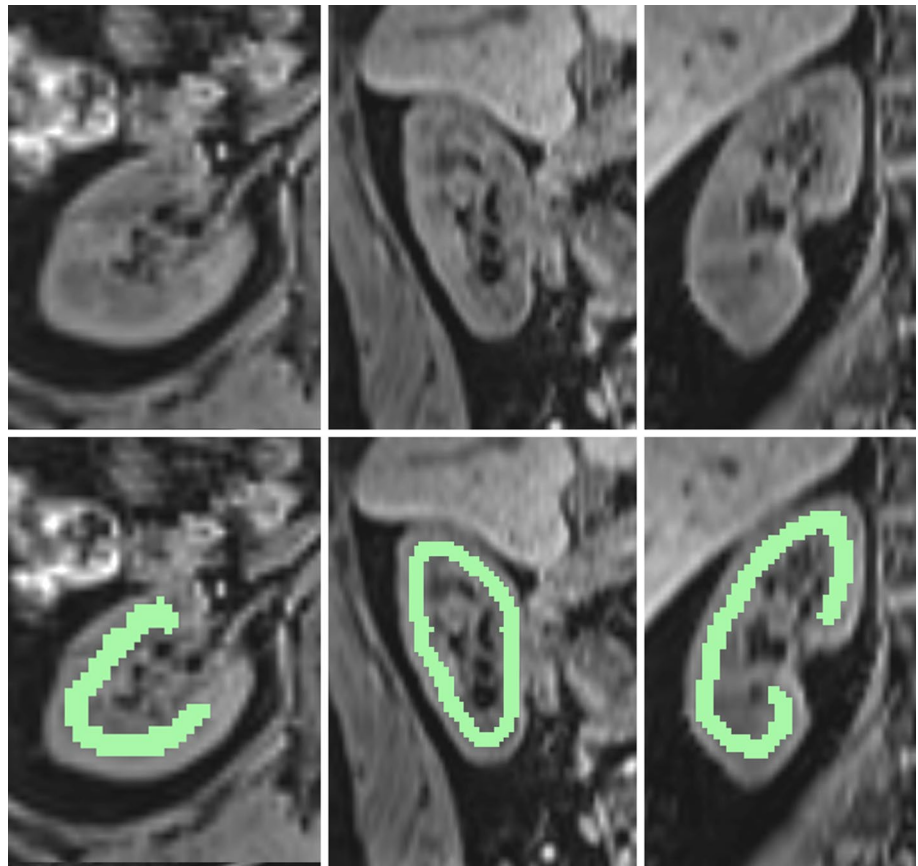
[18]. The tissue characteristics are learned from the user initialization (Fig. 6) and used to guide the active contour evolution. Briefly, RSS computes local robust statistics for 27-voxel neighborhoods of each voxel in the seed region. These statistics include the intensity median, the distance between the first and third quartiles, and signal variance expressed as the median absolute deviation. The estimated probability density function is then used to drive the evolution of closed surfaces while minimizing a two-term energy functional, where the first term measures the similarity of the statistical features for the region and the seed, and the second term is the area of the surface. The output is controlled with three free parameters: the estimated kidney volume, intensity homogeneity (IH), and boundary smoothness (BS), both scalars in the 0.0–1.0 range. The estimated volume was set to 160.6 cm^3, the average volume for our 40 cases.

Generating kidney reference masks

An abdominal radiologist (anonymized for review) with 11 years of experience in renal MRI generated reference masks by free-hand editing of each kidney on each relevant slice. This tedious process used a variable-diameter electronic paintbrush and an eraser, both controlled by the computer mouse. The expert observer used fat-suppressed images to include in the reference masks the renal cortex, medulla and renal cysts (present in 10 % or 4/40 of cases). The renal pelvis, ureter, renal arteries, veins, lymphatic vessels and nerves were excluded. The same radiologist selected four kidneys for parameter optimization.

Optimization of parameters

Images of four kidneys (two left, two right) were used to determine parameters of the algorithm that minimize the average absolute discrepancy D between estimated and reference volumes. Selected cases were deemed to present the most serious problems of separating the kidney from adjacent organs: spleen, liver, intestines, or posterior muscular wall. Optimization was performed in two stages: (1) for fixed $s = 5$, we varied t_{high} (in steps of 0.05) and p and g (in steps of 1 mm); (2) using parameters that best match the reference masks, we then analyzed the effect of s.

Results

Parameter optimization

The minimum error was achieved with $t_{high} = 1.5$, $p = 5$ mm, and $g = 6$ mm. Figure 7 plots D for $s = 5$ and
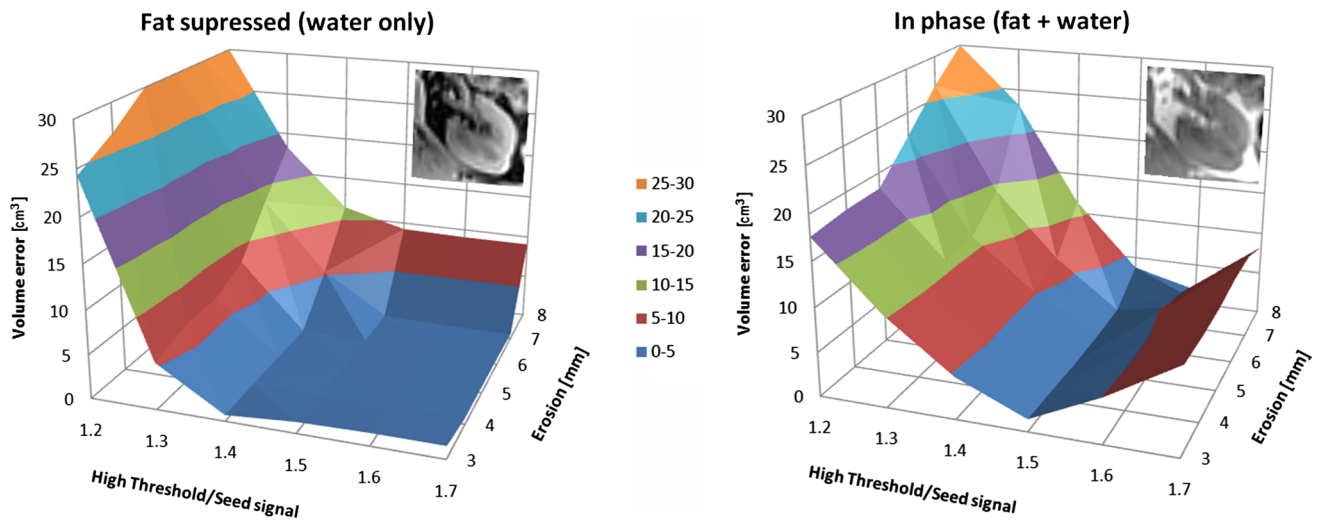
Fig. 7 Error in kidney volume as a function of two key parameters (plotted on the *x* and *y* axes) of the blanket method. See text for the definition of high threshold and erosion parameters. *Left panel* fat-suppressed images; *right panel* original T1-weighted data

a range of the two most sensitive parameters t_{high} and p. Compared with non fat-suppressed images, fat-suppression yielded lower error and a wider plateau of optimal parameters. Consequently, in what follows, we restrict our focus on fat-suppressed images.

The effect of slice skip factor s is shown in Fig. 8. Remarkably, volumetric errors increase on average by only 0.26 % per unit increase in s for s between 4 and 10. The error penalty increases to 1.57 % in the range 10–14. On the other hand, the number of slices traced (right scale in the figure) decreases by an average of 1.56 per unit increase in s in the range 4–10, compared to 0.75 in the range 10–14. Based on this analysis, the remainder of blanket segmentation results are shown for the skip factor $s = 10$.

For the RSS algorithm, the minimum errors were achieved with the combination IH = 0.55 and BS = 0.7.

Accuracy

Manual segmentation (the reference method) of 40 kidneys resulted in a wide range (94.6–254.5 cm^3) of volumes, averaging 160.6 ± 38.3 cm^3. There was no significant difference between the volumes of the left and right kidneys.

Figure 9 plots the volumes assessed by observers against the reference volume. There is a strong linear relationship between the estimated and the true volumes (adjusted $R^2 = 0.97$). The absolute errors in cm^3 were 6.8 ± 5.2 for reader 1 (R1), 4.7 ± 4.4 for R2, and 4.8 ± 3.1 for R3. The relative errors, expressed as % of true volume, were 4.4 % ± 3.0 % for R1, 2.9 % ± 2.3 % for R2, and 3.1 % ± 2.7 % for R3. Figure 10 shows the segmented kidney masks for a representative right and left kidney.
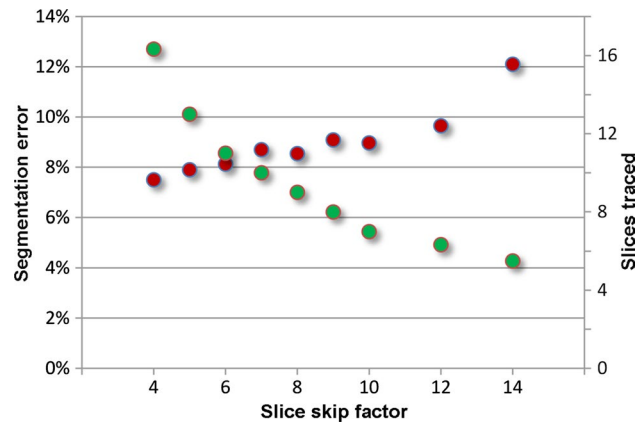

Fig. 8 The effect of slice skip factor s on segmentation error (*red dots*, *left axis*) and on observer effort (*green dots*, *right axis*). The effort is expressed as the average number of slices traced. This number, multiplied by 10-15 s needed to trace one contour, yields the processing time per kidney

Segmentation using the optimized RSS algorithm failed in 9/20 (45 %) of cases. Failure was defined as a grossly inaccurate mask, with volume error >25 %. For the remaining kidneys, errors were 15.4 % ± 6.4 %.

Inter-observer agreement

The average absolute discrepancy between corresponding estimates of kidney volume, i.e., $|V_{ij}-V_{ik}|$, where i indexes the kidneys and j, k represent different readers, was 3.8 ± 3.2 cm^3. The relative discrepancy, $|V_{ij}-V_{ik}|/V_{i,ref}$, where $V_{i,ref}$ is the reference volume, was 2.5 % ± 2.1 %.
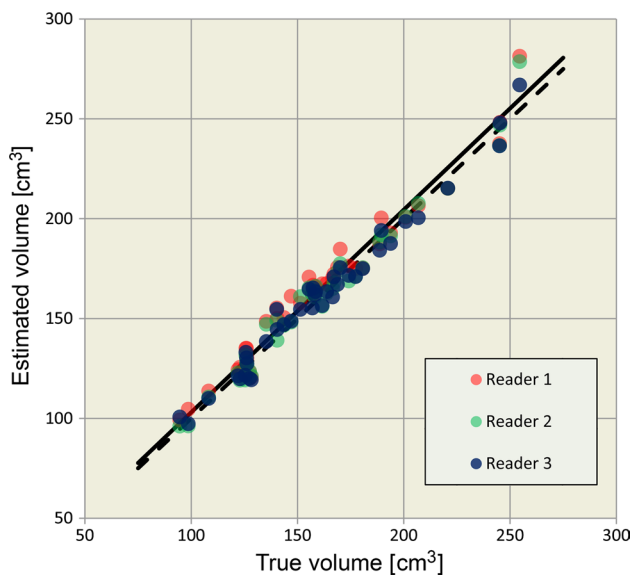
Fig. 9 Volume measured by three readers plotted against the true volume. Also shown are the regression line (*solid*) and the identity line (*dashed*)

Bland–Altman plots (Fig. 11) reveal a small (~4 cm^3) but systematic bias between R1 and the other two readers. Reader agreement does not depend on kidney volume. The range of 95 % agreement (distance between dotted lines in the figure) is ~14.5 cm^3.

After several hours of practice, drawing of blanket regions of interest (ROIs) took between 10 and 15 s per slice. Using the protocol with $s = 10$, or ~7 slices per kidney, this yields an average time of 1.5 min per kidney.

Discussion

Accurate renal segmentation remains a difficult task. Abdominal images suffer from respiratory motion artifacts and signal non-uniformity, and have relatively low signal-to-noise ratios, especially for non-contrast exams. While there is considerable literature on renal segmentation from DCE data [19–21], our focus is on static non-contrast exams. One key decision when setting an abdominal MR protocol is whether to acquire images during a breath-hold
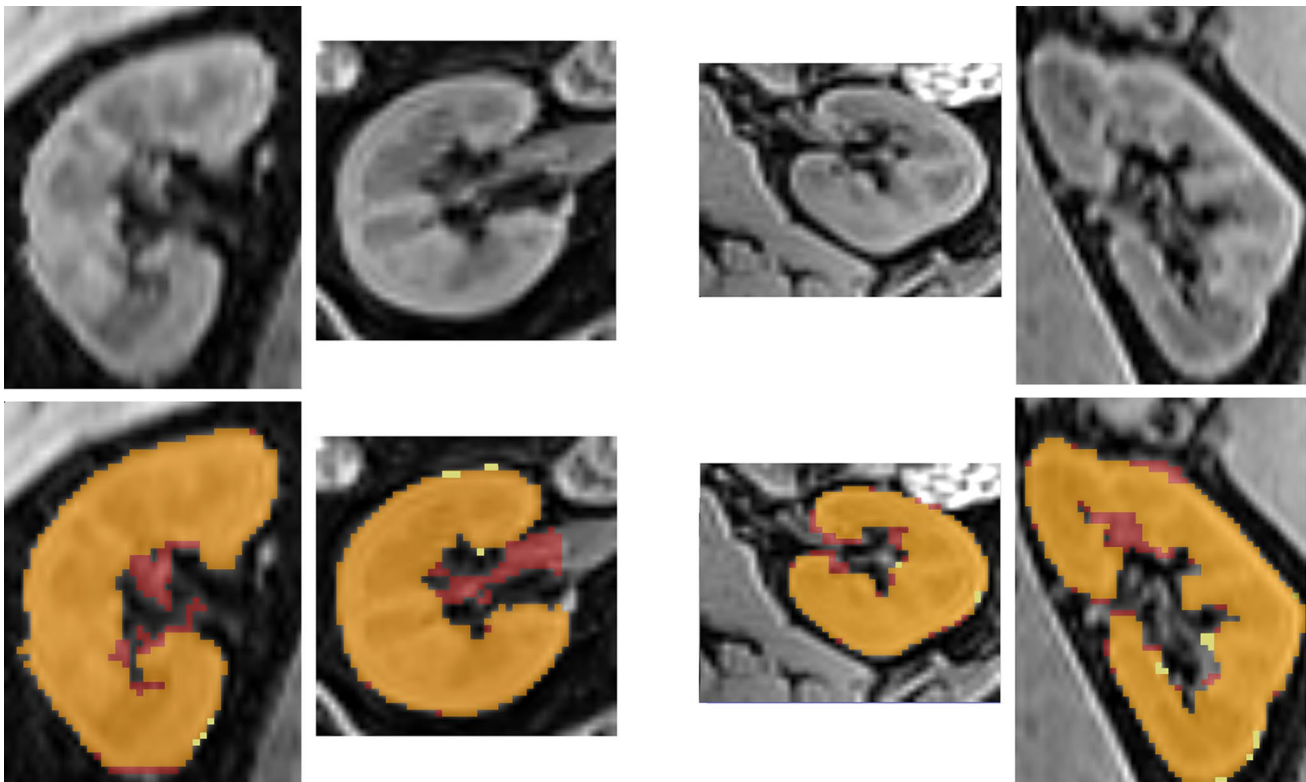

Fig. 10 Examples of over- and under-segmentation errors for a representative right and left kidney. The *top row* shows the original images in coronal and axial views. The segmentation masks are shown on the *bottom*. *Red*: blanket method; *yellow*: reference mask; *orange*: overlap of the two masks. Note over-inclusion of hilar structures in the blanket method
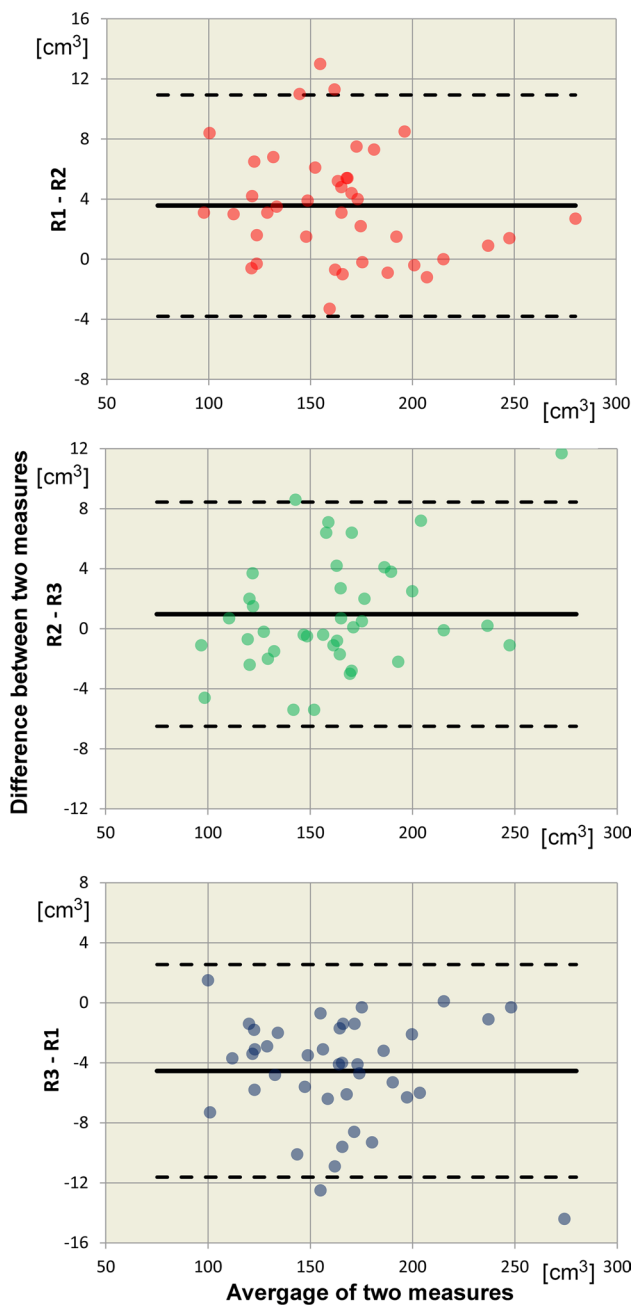
Fig. 11 Bland–Altman plots of the differences between volumes estimated by pairs of readers. *The solid lines* show the mean difference between two readers (the bias), and the *two dotted lines* indicate 95 % limits of agreement (±2 standard deviations around the mean)

themselves to a more robust segmentation, i.e., are less sensitive to the values of segmentation parameters (see Fig. 7) than original in-phase images. Several abdominal organs, including the liver, spleen, paraspinal muscles, and intestines, have similar MR signals and are often in contact with the kidney surface. The area of contact is typically <10 % of the kidney surface. The key concept of the blanket algorithm is to allow a human observer to quickly exclude these organs without affecting the processing of the remaining 90 % of the surface. This idea could be applicable in other medical image segmentation tasks.

Our results confirm that the method is relatively fast and reliable. While we demonstrated high inter-observer agreement, with average absolute discrepancy <3 % across observers, Bland–Altman graphs identified the presence of small systematic inter-observer bias. Observer bias can be reduced by defining clear guidelines about blanket drawing, providing an illustrated list of practical issues, and systematic training.

The level of accuracy and precision achieved in our study compares favorably with the few published methods for the segmentation of kidney MRI without contrast injection. Initial validation of a fully automated segmentation based on combined T1-W and T2-W MRI showed volume errors of 5 % ± 4.1 % [12]. A direct comparison also shows the blanket method to be competitive with the generally available 3D Slicer RSS algorithm [13].

The requirement to draw contours in 10 % of the slices is a clear limitation of the method. On the other hand, this approach provides flexibility, freeing the algorithm from assumption of organ convexity. Another limitation of this study is that the testing was restricted to normal and diabetic kidneys. Future studies are needed to assess the method in other renal diseases and potentially other organs.

Conclusions

We have validated a semi-automated renal segmentation technique that, due to its fast processing speed, high precision, and accuracy, has the potential for implementation in a clinical scenario. Pending further validation, the method could be applied for monitoring of renal status in appropriate patient populations using non-contrast MRI.

Compliance with ethical standards

Conflict of interest The authors declare that they have no conflict of interest.

or to allow for free breathing. Here we opted for a <20-s breath-hold protocol that yields images relatively free of respiratory motion and $2 \times 2 \times 3.8$ mm^3 spatial resolution.

Over most of its surface, each kidney is surrounded by a layer of perinephric fat that provides a bright signal on T1-W images. This signal can be effectively suppressed. Our study suggests that fat-suppressed images lend

References

1. Zöllner FG, Svarstad E, Munthe-Kaas AZ, Schad LR, Lundervold A, Rorvik J (2012) Assessment of kidney volumes from MRI: acquisition and segmentation techniques. AJR Am J Roentgenol 199(5):1060–1069

2. Ellis EN, Steffes MW, Goetz FC, Sutherland DE, Mauer SM (1985) Relationship of renal size to nephropathy in type 1 (insulin-independent) diabetes. Diabetologia 28(1):12–15

3. Baumgartl HJ, Sigl G, Banholzer P, Haslbeck M, Standl E (1998) On the prognosis of IDDM patients with large kidneys. Nephrol Dial Transplant 13(3):630–634

4. Cheung CM, Shurrab AE, Buckley DL, Hegarty J, Middleton RJ, Mamtora H, Kalra PA (2006) MR-derived renal morphology and renal function in patients with atherosclerotic renovascular disease. Kidney Int 69(4):715–722

5. Cheung CM, Chrysochou C, Shurrab AE, Buckley DL, Cowie A, Kalra PA (2010) Effects of renal volume and single-kidney glomerular filtration rate on renal functional outcome in atherosclerotic renal artery stenosis. Nephrol Dial Transplant 25(4):1133–1140

6. George EA, Salimi Z, Wolverson MK, Garvin PJ (1991) Assessment of renal allograft pathology by scintigraphic and ultrasound index-markers. Clin Nucl Med 16(6):394–398

7. Bae K, Park B, Sun H, Wang J, Tao C, Chapman AB, Torres VE, Grantham JJ, Mrug M, Bennett WM, Flessner MF, Landsittel DP, Bae KT (2013) Segmentation of individual renal cysts from MR images in patients with autosomal dominant polycystic kidney disease. Clin J Am Soc Nephrol 8(7):1089–1097

8. Helal I, Reed B, Schrier RW (2012) Emergent early markers of renal progression in autosomal-dominant polycystic kidney disease patients: implications for prevention and treatment. Am J Nephrol 36(2):162–167

9. Goh YS, Wu MW, Tai BC, Lee KC, Raman L, Teo BW, Vathsala A, Tiong HY (2013) Comparison of creatinine based and kidney volume based methods of estimating glomerular filtration rates in potential living kidney donors. J Urol 190(5):1820–1826

10. Rusinek H, Boykov Y, Kaur M, Wong S, Bokacheva L, Sajous JB, Huang AJ, Heller S, Lee VS (2007) Performance of an automated segmentation algorithm for 3D MR renography. Magn Reson Med 57(6):1159–1167

11. Takahashi T, Wang F, Quarles CC (2015) Current MR techniques for the assessment of renal disease. Curr Opin in Nephrol and Hypertens 24(3):217–223

12. Will S, Martirosian P, Wurslin C, Schicket F (2014) Automated segmentation and volumetric analysis of renal cortex, medulla, and pelvis based on non-contrast-enhanced T1- and T2-weighted MR images. Magn Reson Mater Phy 27(5):445–454

13. Gao Y, Kikinis R, Bouix S, Shenton M, Tannenbaum A (2012) A 3D interactive multi-object segmentation tool using local robust statistics driven active contours. Med Image Anal 16(6):1216–1227

14. Pavlidis T (1982) Algorithms for graphics and image processing. Springer, Berlin, pp 174–193

15. Sled JG, Zijdenbos AP, Evans AC (1998) A nonparametric method for automatic correction of intensity nonuniformity in MRI data. IEEE Trans Med Imaging 17:87–97

16. Vivier P-H, Storey P, Chandarana H, Yamamoto A, Tantillo K, Khan U, Zhang JL, Rusinek H, Babb JS, Lee VS (2013) Renal BOLD imaging: contribution of R2 to R2* values. Invest Radiol 48:501–508

17. Mikheev A, Nevsky G, Govindan S, Grossman R, Rusinek H (2008) Fully automatic segmentation of the brain from T1-weighted MRI using Bridge Burner algorithm. J Magn Reson Imaging 27(6):1235–1241

18. Pieper S, Halle M, Kikinis R (2004) 3D Slicer. In: Proceedings of IEEE international symposium biomed imaging, 632–635

19. Woodard T, Sigurdsson S, Gotal JD, Torjesen AA, Inker LA, Aspelund T, Eiriksdottir G, Gudnason V, Harris TB, Launer LJ, Levey AS, Mitchell GF (2015) Segmental kidney volumes measured by dynamic contrast-enhanced magnetic resonance imaging and their association with CKD in older people. Am J Kidney Dis 65(1):41–48

20. Zöllner FG, Sance R, Rogelj P, Ledesma-Carbayo MJ, Rørvik J, Santos A, Lundervold A (2009) Assessment of 3D DCE-MRI of the kidneys using non-rigid image registration and segmentation of voxel time courses. Comput Med Imaging Graph 33(3):171–181

21. Tang Y, Jackson HA, De Filippo RE, Nelson MD, Moats RA (2010) Automatic renal segmentation applied in pediatric MR urography. Int J Intell Inf Process 1(1):12–19